Hindawi
Advances in Civil Engineering
Volume 2019, Article ID 2375276, 16 pages
https://doi.org/10.1155/2019/2375276

Research Article

Experimental Investigation on Dynamic Fracture Mechanism and Energy Evolution of Saturated Yellow Sandstone under Different Freeze-Thaw Temperatures

Liang Chen,[1,2] **Xianbiao Mao**,[1,2] **Shengli Yang**,[3] **Chao An**,[1,2] **and Peng Wu**[1,2]

[1]*State Key Laboratory for Geomechanics and Deep Underground Engineering, China University of Mining & Technology, Xuzhou 221116, China*
[2]*School of Mechanics and Civil Engineering, China University of Mining & Technology, Xuzhou 221116, China*
[3]*School of Energy and Mining Engineering, China University of Mining & Technology, Beijing 100083, China*

Correspondence should be addressed to Shengli Yang; yangsl@cumtb.edu.cn

Received 19 June 2019; Revised 21 August 2019; Accepted 6 September 2019; Published 13 October 2019

Academic Editor: Eric Lui

The coupling effect of freeze-thaw (F-T) temperature and dynamic load on the dynamic mechanical properties and fracture mechanism of saturated yellow sandstone was experimentally investigated in this research. The dynamic compression tests on the specimen after different F-T temperatures (i.e., −5°C, −10°C, −15°C, −20°C, −30°C, and 20°C) have been carried out with split-Hopkinson pressure bar (SHPB) setup under eight F-T cycle numbers. The density and *P*-wave velocity of the specimens were obtained before and after the F-T tests. After the F-T tests, the specimen microstructures were examined via the scanning electron microscope (SEM). The dynamic fracture process was visualized by the high-speed camera. The particle size distribution and fragment shapes of the specimens were analyzed using a classifying screen. In addition, the energy dissipation law of specimens during the impact test was also discussed. Experimental results show that the dynamic elastic modulus, strength of the specimen, and the average particle size decrease with decreasing F-T temperature. SEM results reveal that low F-T temperature leads to severer internal damage of the specimen by inducing freeze-swell holes, interconnected cracks, and pore clusters. In addition, the fragmentation shapes of the failed specimens exhibit double-cone failure, single-side slope failure, double-side slope failure, and split failure. The energy dissipation increases gradually with increasing F-T temperature. This study helps to prevent geological disasters and optimize engineering design in cold regions.

1. Introduction

The mechanical properties and fracture behavior of intact rock have a big influence on engineering reliability and stability in mining and civil engineering projects [1]. These behaviors may be influenced by many factors such as external environment, loading conditions, and microstructures of intact rocks [2–7]. Among them, the freeze-thaw (F-T) effect is one of the most representative external environmental factors. The distribution area of permafrost and seasonal frozen regions accounts approximately 23% of the world's total land area [8]. With the development of engineering constructions in cold regions, the design and maintenance of these engineering requires a more profound understanding for the mechanical properties and fracture mechanism of rocks under complex thermal-mechanical conditions. In some special cases, excavation works in cold region include blasting and other forms of the impact load. For instance, rock slopes in open pit mines and tunnel concrete coating located in cold region are subjected to the deterioration caused by the coupling effects of impact load and F-T effect. Thus, a thorough understanding on the mechanical and fracture behavior of rocks under dynamic load after F-T treatment seems to be crucial for the safety and stability of rock engineering in cold region engineering.

The change in mechanical behavior is caused by the rock pore structure deterioration under F-T conditions. In previous works, some attempts have been made to investigate

the degradation and fracture behavior of F-T treated rocks [9–16]. However, most of the previous reports mainly focused on the static mechanical research [17, 18]; and only a few studies on coupled dynamic mechanical deterioration and fracture behavior have been reported. Wen et al. [19] discussed the relationship between dynamic mechanical strength and the number of F-T cycles using the experimental and LS-DYNA numerical simulation methods. They found that the peak strength and the slope of the postpeak stress-strain curve of samples were different before and after F-T cycles. Yang et al. [20] carried out the dynamic mechanical testing on sandstone subjected to F-T cycles and analyzed the evolution characteristics of peak strength, peak strain, and dynamic stress-strain curve of the specimen with the changing number of F-T cycles. From the microscopic perspective, Zhou et al. [21] investigated the effect of F-T cycles on the microscopic damage and dynamic mechanical properties of sandstone. The studies by Ke et al. [22] show that the pore structure obviously changed with increasing F-T cycles and then an evolution equation for predicting the dynamic peak strength of sandstone after F-T cycles was put forwarded. Based on the above summary, it is clear that the number of F-T cycles was taken as a variable to study rock mechanical and fracture behavior in cold region engineering [23]. However, there are limited reports in the literature which focus on the coupled effect of impact loading and F-T temperature on the mechanical and fracture behavior of rocks [17, 24].

As shown in Figure 1, it indicates a clear temperature distribution from −12°C in the south region to −28°C in the north region during winter, of which these areas cover more than 85% of the total area in China. Hence, it is important to consider the temperature fluctuations in engineering design for preventing the occurrence of dynamic disasters in cold regions. In relevant literature, Liao et al. [25] carried out the impact test on dry and saturated sandstone under different low temperatures and investigated the relationship between dynamic mechanical properties, temperature, and moisture content under low-temperature condition. The results show that the change law of saturated specimen peak strength is initially increasing slowly and then dropping sharply in the temperature range of 25°C to −40°C with the turning point temperature at −30°C. Meanwhile, the trend of peak strain is initially dropping rapidly and then increasing sharply with the turning point temperature at −10°C. This work mainly focuses on the following four aspects: (1) How does the F-T temperature affect the dynamic mechanical parameters of rocks subjected to the same strain rate? (2) How does the F-T temperature damage the internal structure of rocks after F-T treatment? (3) What is the relationship between F-T temperature and particle size distribution of specimens after impact test? and (4) How does the F-T temperature affect the energy dissipation law of specimens?

Based on the above research interests, the mechanical and fracture behavior of yellow sandstone under the coupling effect of F-T temperatures and impact load is investigated through the split-Hopkinson pressure bar (SHPB) at eight F-T cycles. A high-speed camera is used to capture the fracture process of the specimens. The macroscopic and microscopic fracture morphology and the mechanical properties under different F-T temperatures are discussed.

2. Experimental Study

2.1. Rock Specimen Preparation. As shown in Figure 1, the rock specimens are yellow sandstone collected from the Haerwusu open-pit coal mine in Inner Mongolia of China. According to the requirements of rock dynamic mechanics experiments, the specimens (shown in Figure 2) are prepped and cored into cylinders which have a diameter of 50 mm and a height of 25 mm with the errors of height and diameter less than 0.05 mm and 0.02 mm, respectively [26]. In addition, the uniaxial compression tests are carried out at 20°C, and the basic mechanical parameters as well as stress-strain curve of rock specimens are shown, respectively, in Table 1 and Figure 3. It can be seen that the average *P*-wave velocity and density of the specimen are 2451 m/s and 2329 kg/m^3 with the average uniaxial compressive strength of 32.93 MPa and Young's modulus of 4.40 GPa.

2.2. F-T Experimental Equipment and Procedure. Moisture content is an important factor affecting the physical and mechanical properties of rock mass during F-T process [9]. To eliminate the effect of moisture content, the yellow sandstone is first fully saturated before carrying out the F-T tests. The specimens undergo the F-T treatment through the JC-ZDR-5 automatic low-temperature testing machine, which is mainly composed of the temperature control system, F-T cycle tank, and refrigeration compressor (Figure 4(b)). The freezing temperature, F-T time, and the F-T cycle number can be automatically adjusted by the operating panel of the temperature control system. The experimental procedure is as follows:

(i) First, the *P*-wave velocity of natural samples is measured by the *P*-wave velocity monitoring system (Figure 4(a)) and then the specimen with similar wave velocities is selected and divided into six groups with three specimens in each group. The selected specimens are dried in an incubator for 24 hours at 105°C and then placed in a sealed tank to extract gas with water injection for 12 hours until the bubble-free overflow from the surface of the specimen.

(ii) Then, the air pressure is adjusted in the sealed tank to the atmospheric pressure and kept for 12 hours. It can be considered that rock samples are fully saturated as the saturated moisture content was found to be 3.17%. The saturated samples are placed in the F-T cycle tank (Figure 4(b)) and frozen at different temperatures (−5, −10, −15, −20, and −30°C) with eight F-T cycles. The number of F-T cycles in this experiment is consistent with the seasonal F-T cycles number of the slope located in the Haerwusu open-pit coal mine. The detailed F-T test process is shown in Figure 5 in which the freezing and thawing time are both 6 hours.

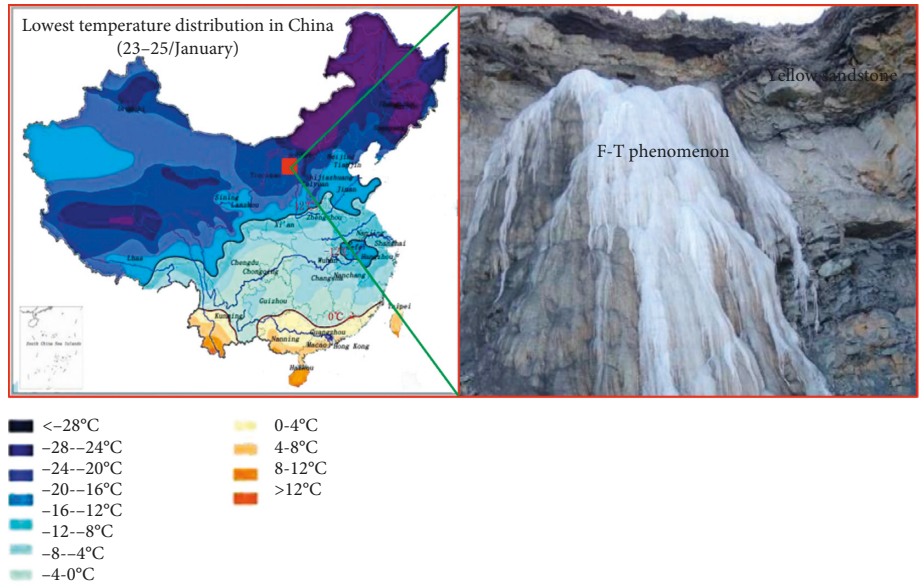

Figure 1: Cold region distribution in China.

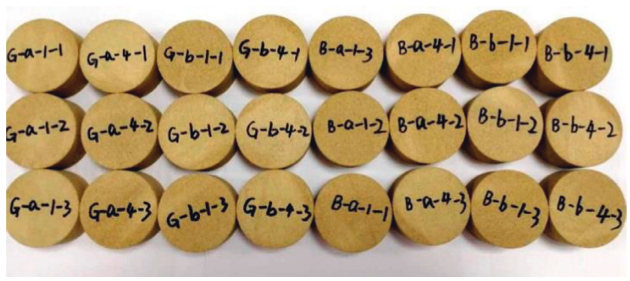

Figure 2: Yellow sandstone samples in this study.

(iii) Finally, the *P*-wave velocity of specimens after the F-T treatment is measured again, and the microstructural characteristics of specimens will be observed by scanning electron microscope (SEM) after F-T treatment (Figure 4(d)).

2.3. Impact Experimental Equipment and Procedure. As shown in Figure 6, the impact tests are carried out on a 50 mm diameter SHPB test system, which consists of a loading drive device, pressure bar device, energy absorption device, a signal acquisition, and analysis device. During the impact test, the specimen is initially placed between the incident bar and transmission bar, and then an impact loading is applied by colliding the striker bar with the incident bar. This impact will form an incident pulse or stress plus in the incident bar which will be transmitted to the free end of the rock sample. The stress pulse will be reflected and transmitted many times at the specimen-incident bar or specimen-transmission bar interface and cause high-speed compression deformation of specimens. Some incident pulses are returned to the incident bar as reflected pulse, while others are transmitted to the transmission bar as transmitted pulse. The pulses will be recorded into a signal acquisition system by the strain gauge on the elastic compression bar. Finally, the whole deformation process of the specimen will be recorded by the millisecond high-speed camera for analyzing the macroscopic failure process of yellow sandstone. The experimental procedure is as follows:

Table 1: Physical and mechanical properties of yellow sandstone (50 mm × 100 mm).

Samples	ρ (kg·m^{-3})	v (m·s^{-1})	σ_c (MPa)	E (GPa)	ε_c (%)
1#	2330	2450	34.32	4.64	1.31
2#	2324	2463	31.01	4.21	1.28
3#	2332	2441	33.46	4.35	1.35
Average value	2329	2451	32.93	4.40	1.31

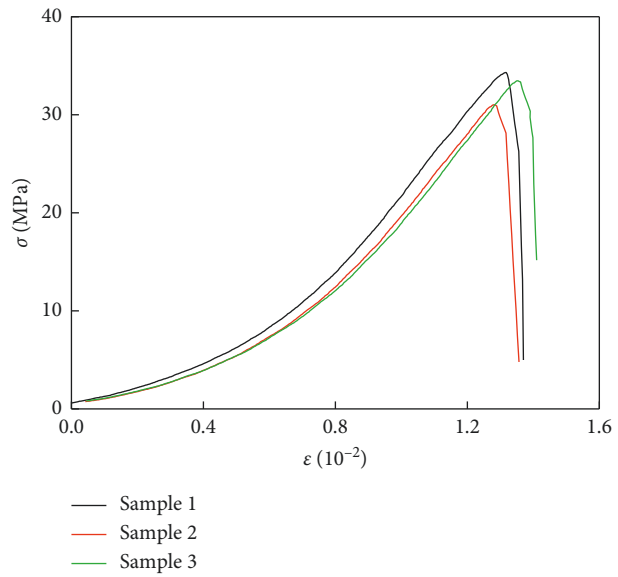

Figure 3: Uniaxial compression stress-strain curve of yellow sandstone.

Figure 4: Testing systems in this work. (a) *P*-wave velocity monitoring system. (b) Freeze-thaw cycle equipment. (c) Impact loading test equipment. (d) SEM device. (e) Classifying screen.

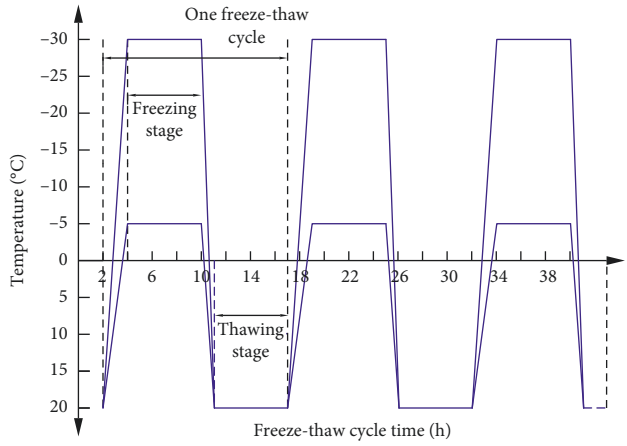

Figure 5: Temperature profile of the yellow sandstone samples undergoing the F-T cycle.

(i) Firstly, the impact tests of specimens under normal temperature are carried out by using the SHPB test system (Figure 4(c)) at the pressure range of 0.2–0.40 MPa. Then, it can be inferred from the fragments collected after the impact test that the fracture degree of specimens is severe when the air pressure reaches 0.35 MPa and has a smaller change with the gradually increase in air pressure. Hence, the air pressure 0.35 MPa is selected as an impact loading in this experiment. The typical shaped waveform measured in SHPB test is shown in Figure 7.

(ii) Then, a series of impact tests are carried out to study the dynamic mechanical and fracture behavior of saturated yellow sandstone after F-T. During the impact test, the striker bar velocity is measured by a speedometer at different F-T temperatures; meanwhile, the strain rates of specimens are obtained

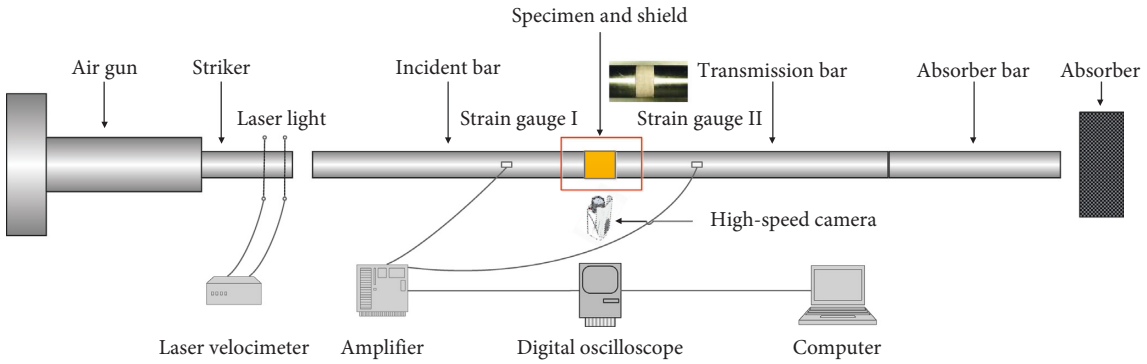

Figure 6: Structural characteristic of the SHPB.

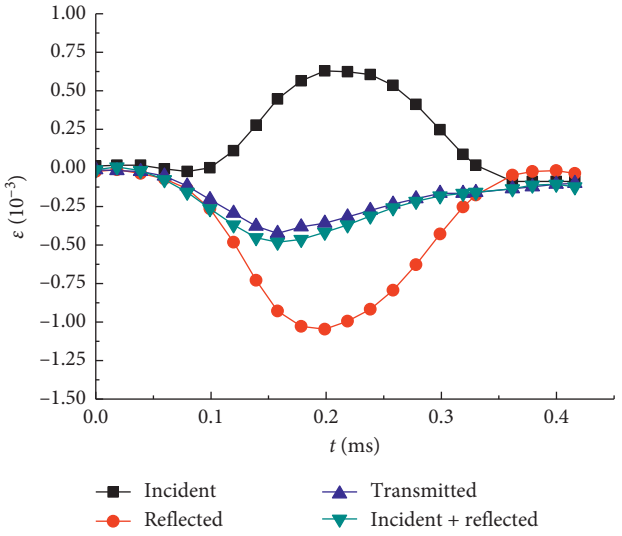

Figure 7: Typical shaped waveform.

using a three-wave method [27]. The striker bar velocity and the strain rate in this experiment are shown in Table 2. It can be seen that their values change with varying F-T temperatures. The average striker bar velocity ranges from 9.33 m/s to 9.67 m/s under the same impact load, indicating a relatively stable loading condition. In addition, the average strain rates are in the range of 72.88 s^{-1} to 75.97 s^{-1}, indicating the consistency at different temperatures.

(iii) Finally, the specimen fragments are collected after impact tests and then the particle size is also counted by using a classifying screen (Figure 4(e)).

3. Experimental Results Analysis

3.1. Influence of F-T Temperatures on Physical Parameters of Yellow Sandstone. Figure 8 shows the variation in the *P*-wave velocity (v) and the density (ρ) of yellow sandstone with varying F-T temperatures. It is noted that all data reflect the average values of the physical parameters of yellow sandstone. According to Figure 8, the F-T temperature has an extremely important effect on the *P*-wave velocity and density of the yellow sandstone. Compared with the normal temperature, v and ρ decreased by 35.58%~49.69% and 34.52%~50.11% from −10°C to −30°C, respectively. In addition, the *P*-wave velocity increased linearly as the F-T temperature rises, whereas the specimen density increased nonlinearly.

Table 2: Velocity of striker bar (v) and strain rate of specimen ($\dot{\varepsilon}$) under different freezing temperatures.

Sample	T (°C)	v (m·s^{-1})		$\dot{\varepsilon}$ (s^{-1})	
		Each sample	Average value	Each sample	Average value
1	20	9.53	9.51	74.34	74.74
2		9.69		76.98	
3		9.31		72.87	
4	−5	9.25	9.49	71.47	74.57
5		9.49		74.88	
6		9.72		77.37	
7	−10	9.81	9.51	78.69	74.89
8		9.33		72.16	
9		9.39		73.81	
10	−15	9.54	9.33	74.23	72.88
11		9.19		71.59	
12		9.27		72.82	
13	−20	9.71	9.67	76.80	75.97
14		9.77		77.61	
15		9.54		73.50	
16	−30	9.71	9.54	73.92	73.60
17		9.74		75.26	
18		9.17		71.63	

3.2. Influence of F-T Temperatures on Dynamic Stress-Strain Curve. The dynamic stress-strain curves under various F-T temperatures are shown in Figure 9. Figure 10 illustrates the typical dynamic stress-strain curve and fracture process of the yellow sandstone. The stress-strain curve first experiences a very short nonlinear deformation where the initial pores and microcracks are compressed under the effect of impact loading. Afterwards, the stress-strain curve shows linear change, indicating the rock mass enters the dynamic elastic stage where no new microcracks propagated. Later, the stress-strain curve starts to nonlinear

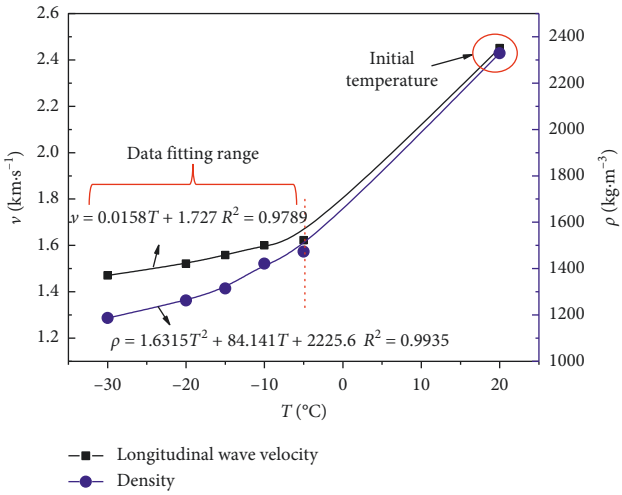

Figure 8: Relationship between physical parameters and F-T temperatures.

increase with the decreasing deformation speed rate, indicating that the new microcrack within the rock appears and gradually propagates to the rock surface. Finally, the specimen enters the postpeak stage where splitting and shear failure occur with the appearance of macroscopic cracks. The yellow sandstone deformation features the following stages considering the influence of F-T temperatures: (1) dynamic compaction stage, (2) elastic stage, (3) dynamic hardening stage, and (4) postpeak attenuation stage. Comparing with the dynamic stress-strain curve under the normal temperature, the F-T temperature has considerable effect on the curve characteristic of specimen, i.e.,

(i) An obvious dynamic compaction stage after F-T treatment. As the F-T temperature is decreased from −5°C to −30°C, the percentage of dynamic compaction stage gradually increases in the prepeak region of the curve. However, there is no obvious dynamic compression under the normal temperature (20°C). It maybe because the internal cracks and pores of specimens after F-T treatment gradually increase compared with the normal temperature, resulting in a relatively obvious dynamic compression stage. The research results in Section 5 can support the viewpoint.

(ii) The phenomenon of postpeak strain softening appears for all the curves when the specimens are exposed to various F-T temperatures. However, the stress-strain curves from 20°C to −20°C drop rapidly after dynamic hardening stage. When the F-T temperature arrived −30°C, the attenuation slope of the postpeak stress strain curve slightly decreases. It means that the ductility of the yellow sandstone gradually increases.

(iii) The strength parameters of the rock mass, such as dynamic Young's modulus (E_d), dynamic peak strength (σ_d), and dynamic peak strain (ε_d), varied as the F-T temperature changed.

3.3. Influence of F-T Temperature on Dynamic Mechanical Properties. As shown in Figure 9, the dynamic Young's modulus, dynamic peak strength, and dynamic peak strain can be obtained as shown in Table 3.

The dynamic elastic modulus reflects the deformation resistance of the specimen exposed to F-T treatment. In general, there are many various methods to determine elastic modulus, which mainly include secant modulus, tangent modulus, average modulus, and so on. In this work, we take the straight line slope of the stress-strain curve in elastic stage as the elastic modulus of the specimen. The methods have already been used in other papers [28]. Figure 11 depicts the relationship between the dynamic elastic modulus (E_d) and the F-T temperatures (T). Generally, dynamic Young's modulus decreases with decreasing F-T temperature. For instance, the parameter E_d decreases by 54.91% (from 27.57 GPa to 12.43 GPa) when the F-T temperature decreases from −10°C to −20°C and then only decreases by 46.74% (from 12.43 GPa to 6.62 GPa) when the F-T temperature drops from −20°C to −30°C. It means that the lower the F-T temperature, the weaker the deformation resistance of the yellow sandstone under the same F-T cycle number.

The dynamic peak strength (σ_d) and peak strain (ε_d) represent the ultimate bearing capacity and deformation behavior of the yellow sandstone, respectively. Figure 12 reveals the relationships between the two parameters (σ_d and ε_d) of the yellow sandstone and the F-T temperature. As the F-T temperature decreases, the dynamic peak strength decreases linearly, whereas the dynamic peak strain increases linearly. When the F-T temperature drops from −10°C to −30°C, the dynamic peak strength is reduced from 61.97 MPa to 37.51 MPa with a considerable drop of 39.47%. Moreover, the dynamic peak strain increases from 0.91% to 1.42% with an increase rate of 56.04%. It means that the yellow sandstone specimen experiences brittle behavior to ductile behavior transition as the F-T temperature decreased. The ultimate bearing capacity of specimens also gradually dropped.

4. Lumpiness Distribution

4.1. Effect of F-T Temperature on the Particle Size. The lumpiness distribution reflects the macroscopic fracturing of the specimen under different F-T temperatures. The lumpiness distribution can be expressed by the average particle size of the specimen. The typical lumpiness distribution and cross-section morphology of the yellow sandstone under different F-T temperatures are shown in Figures 13 and 14, respectively. The particle sizes of each specimen can be divided into eight groups through a classifying screen. The gradient range of particle sizes are 0–1, 1–2.5, 2.5–4, 4–6, 6–8.5, 8.5–11, 11–13, and >13 mm, and they are represented by the notations 8, 7, 6, 5, 4, 3, 2, and 1, respectively. The different particle size mass, W_n, of the same specimen can be measured by the high-precision electronic balance. The mass percentage, W_{sn}, of each particle size to the total mass can be calculated. In Figure 15, it should be noted that W_{sn} is the average values from multiple test samples under the same experimental conditions.

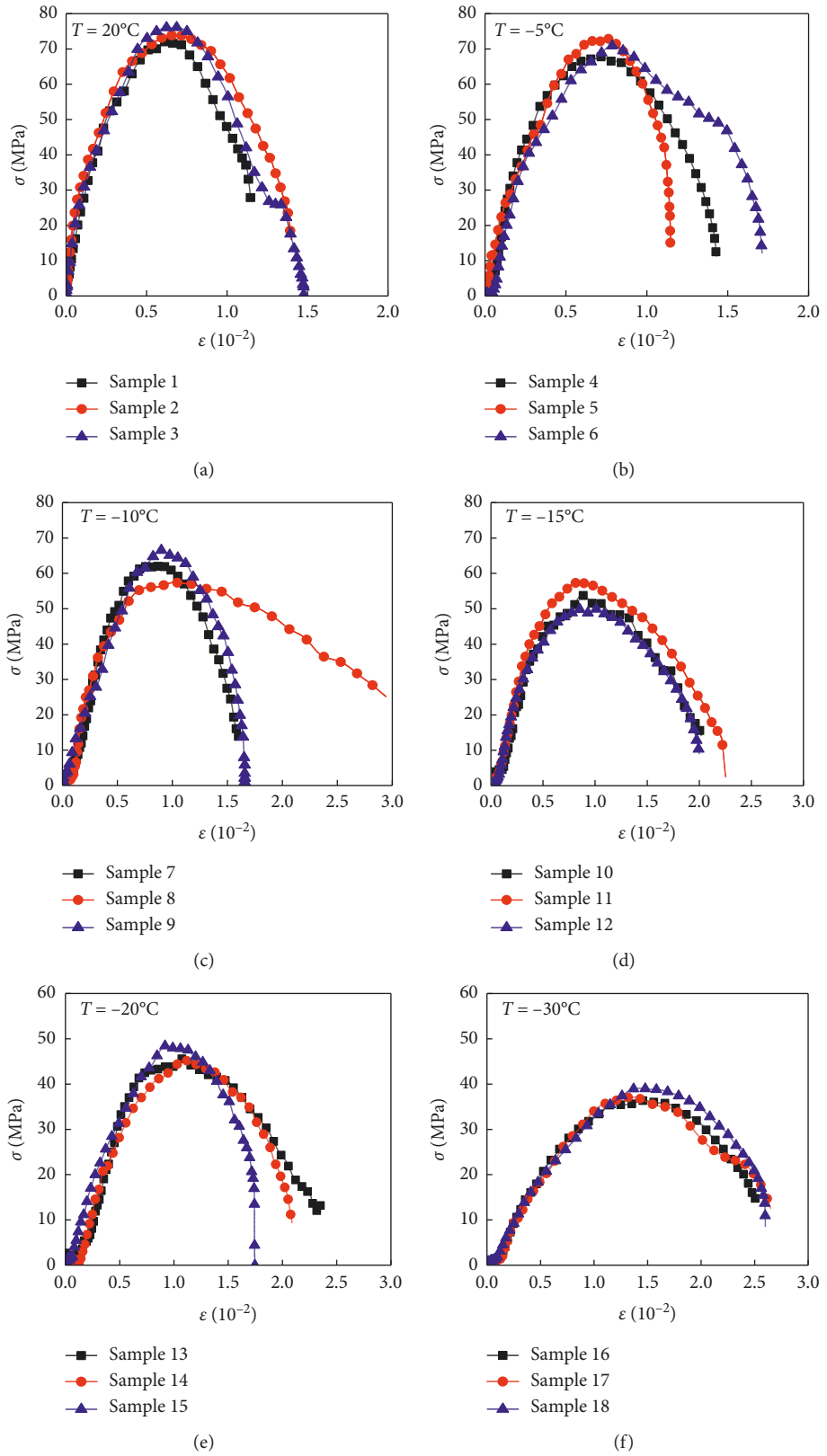

Figure 9: Dynamic stress-strain curves under various F-T temperatures.

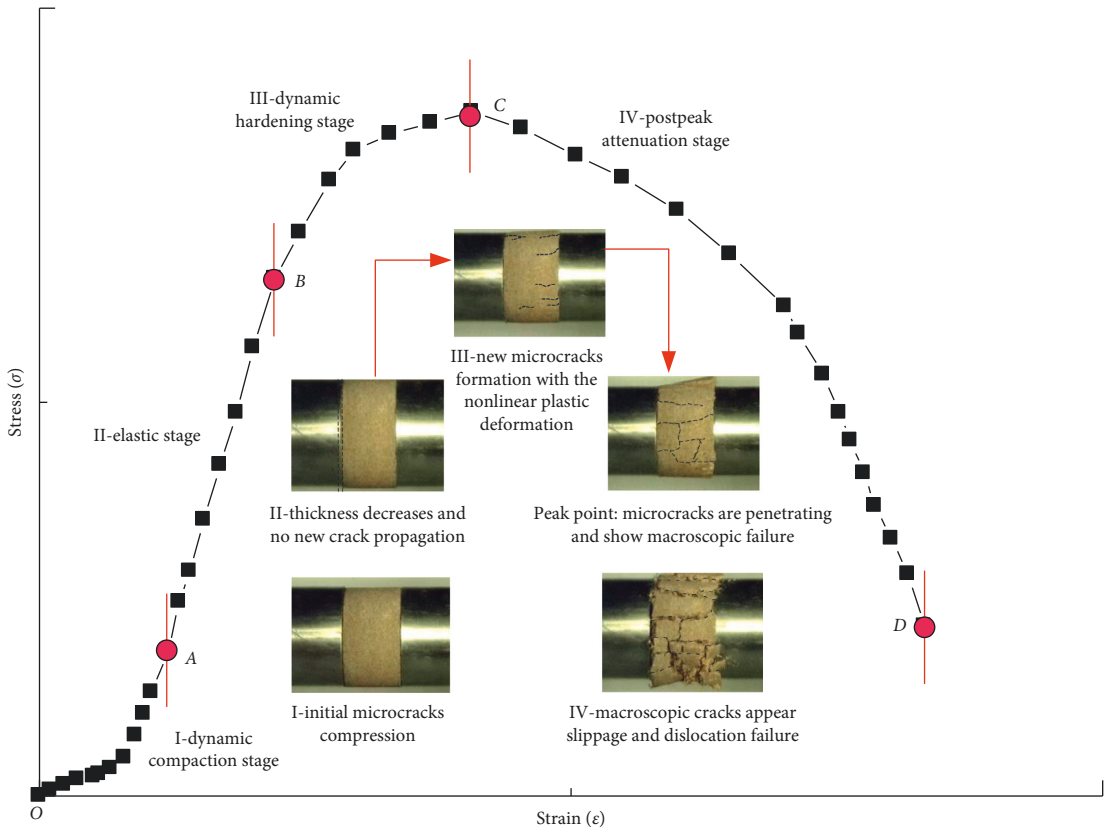

Figure 10: Typical dynamic stress-strain curve and fracture process of yellow sandstone.

Table 3: Dynamic elastic modulus (E_d), peak strength (σ_d), and peak strain (ε_d) under different freezing temperatures (σ_d is the peak stress of dynamic stress-strain curve; ε_d is the strain corresponding to the peak stress; and E_d is the slope of the stress-strain curve in elastic stage).

Specimen	T (°C)	E_d (GPa)		σ_d (MPa)		ε_d	
		Sample	Average	Sample	Average	Sample	Average
1		36.71		72.06		0.0062	
2	20	38.42	38.29	73.94	74.02	0.0068	0.0064
3		39.73		76.05		0.0063	
4		37.21		67.73		0.0072	
5	−5	30.79	34.00	72.88	70.49	0.0075	0.0075
6		35.82		70.86		0.0079	
7		28.74		62.10		0.0087	
8	−10	29.78	27.57	57.38	61.97	0.0101	0.0091
9		24.19		66.52		0.0085	
10		17.13		53.78		0.0089	
11	−15	20.37	19.07	57.55	53.74	0.0086	0.0093
12		19.72		49.90		0.0104	
13		12.67		45.58		0.0108	
14	−20	13.04	12.43	45.26	46.44	0.0110	0.0104
15		11.58		48.49		0.0093	
16		6.85		36.35		0.0147	
17	−30	6.52	6.62	37.12	37.51	0.0136	0.0142
18		6.49		39.07		0.0142	

Figure 13 indicates that the rock fragments can be roughly divided into two types: the main fragment and secondary fragment in all fractured specimens when the strain rate is in the range of 72.88 s^{-1}~75.97 s^{-1}. The cross section of the main fragment always display an obvious circular grooves in the middle of maximum particle size block no matter what the F-T temperature is, which is termed the double-cone-failure pattern. The secondary fragment mainly includes the double-side slope pattern, single-side slope pattern, and split failure pattern. Technically, both the slope-failure pattern and

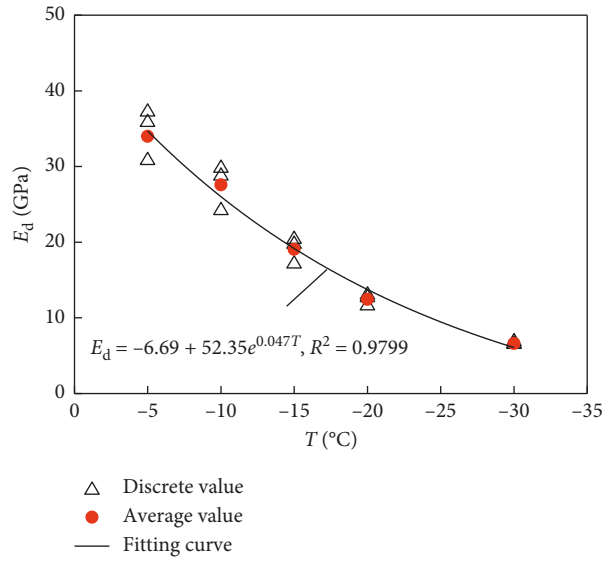

Figure 11: Relationship between dynamic elastic modulus (E_d) and F-T temperatures (T).

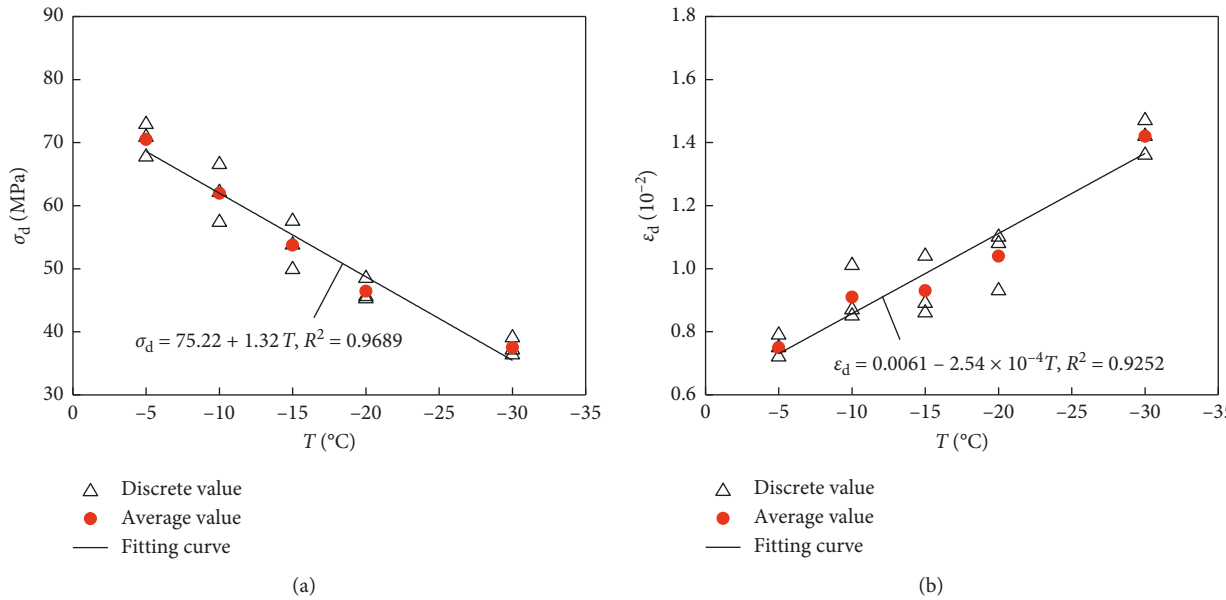

Figure 12: Dynamic peak strength (σ_d) and peak strain (ε_d) change curve with F-T temperatures (T).

double-cone-failure pattern belong to the modes of shear failure [29]. Therefore, the yellow sandstone presents the split-shear combined failure form. As shown in Figure 15, the mass percentage of minimum size particles ($n = 8$) gradually increases with decreasing F-T temperature. On the contrary, the mass percentage of maximum size particles ($n = 1$) decreases.

To quantify the influence of the F-T temperature on the fracture degree of the yellow sandstone, the particle size coefficient r is introduced to represent the average particle size of the specimen [28]:

$$r = \sum_{n=1}^{8} W_{sn} d_{ms}, \tag{1}$$

where d_{ms} is the average particle size in each particle size range. When $n = 1$, the minimum and maximum particle sizes are, respectively, 13 mm and 50 mm. The larger the particle size coefficient is, the larger the average particle size is, which means that the fracture degree of the specimen is lower.

Table 4 shows the value of particle size coefficients under different F-T temperatures. Figure 16 shows the relationship curve between particle size coefficient, r, and the F-T temperature, T. As the F-T temperature rose from −30°C to −20°C or from −5°C to 20°C, the particle size coefficient gradually increases with a smaller speed rate. However, when the F-T temperature rose from −20°C to −5°C, the particle size coefficient rapidly increased nonlinearly. For instance,

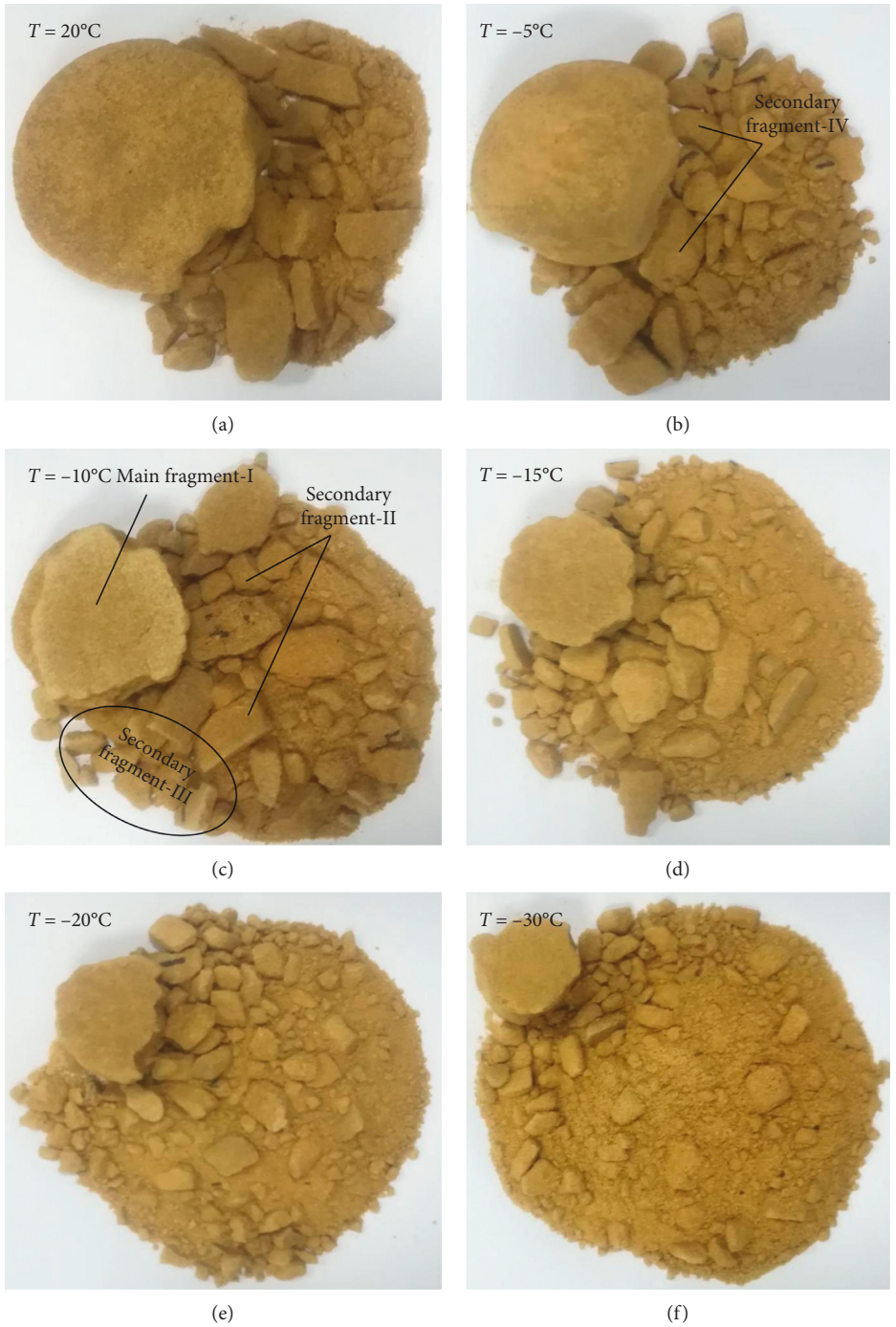

Figure 13: Typical lumpiness distribution characteristic of yellow sandstone under different F-T temperatures.

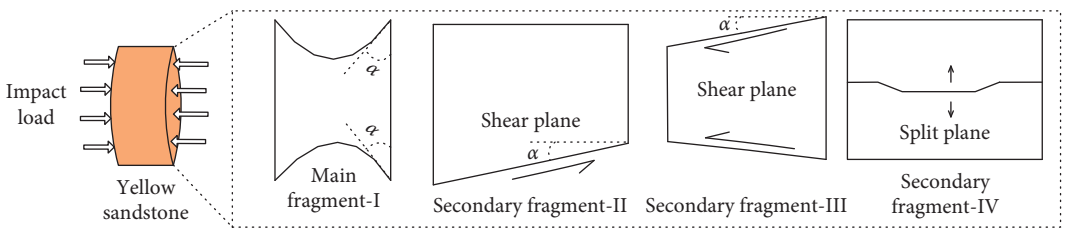

Figure 14: Typical cross-section morphology of yellow sandstone after impact fracture. Fragment I, double-cone-failure; fragment II, single-side slope failure; fragment III, double-side slope failure; fragment IV, split failure.

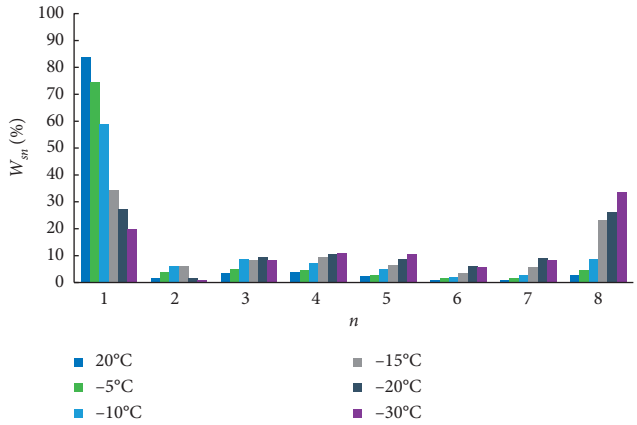

Figure 15: Mass percentage of different particle size fragments under different F-T temperatures.

Table 4: Particle size coefficients under different F-T temperatures.

T (°C)	20	−5	−10	−15	−20	−30
r (mm)	15.27	14.24	12.55	8.72	7.46	6.15

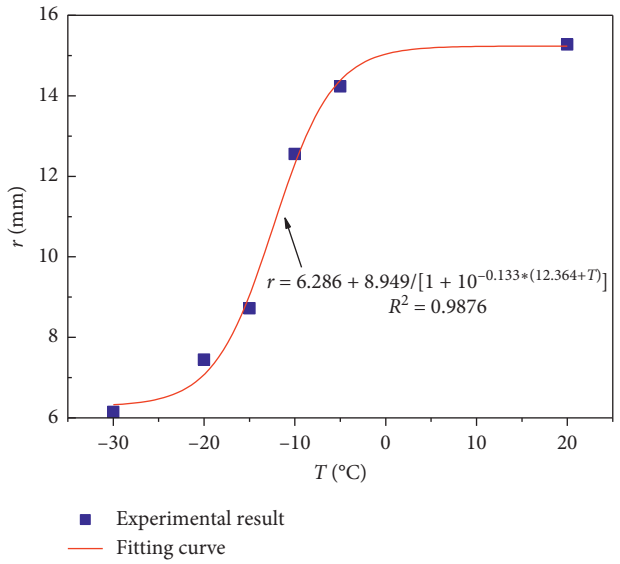

Figure 16: Relationship curve between particle size coefficient and F-T temperatures.

when the F-T temperature increased from −30°C to −20°C or from −5°C to 20°C, the particle size coefficient only increased 1.31 mm with an increase of 21.3% or 1.03 mm. When the F-T temperature grew from −20°C to −10°C, the particle size coefficient rapidly increased to 5.09 mm with a significant rise of 68.23%. Thus, the F-T temperature strongly affects the lumpiness distribution (fracture degree) of the yellow sandstone, particularly in the range of −20°C to −5°C. The lower the F-T temperature, the higher the dynamic damage degree of rock.

Actually, the trend of particle size coefficient with increasing F-T temperature is different from the mechanical parameters (σ_d, E_d, ε_d). It may be because that the number of microcracks may not be the only factor related to the fracture degree of specimens. In addition, the distribution form and propagation direction are also influencing the trend. As shown in Figure 17, the main crack and interconnected crack begin to appear in large scale when the temperature is below −10°C, which may increase the fracture degree of the specimens. As a result, the relationship curve between particle size coefficient and F-T temperatures shows a sharp decreasing trend.

4.2. Discussion on Relationship among Particle Size Coefficients and Mechanical Parameters. Figure 18 indicates that the relationship among particle size coefficient and elastic modulus as well as peak strength. Figure 19 shows the change trend of peak strain with the particle size coefficient. It can be seen from Figures 18 and 19 that the elastic modulus and peak strength approximately linear increase with increasing particle size coefficient, respectively, whereas the peak strain gradually decreases nonlinearly. It means that the change in mechanical parameters caused by F-T temperature is closely related to the fracture degree of specimens reflected by the particle size coefficient. In open-pit mines, we may be able to optimize blasting parameters in advance by the methods of using dynamic mechanical parameter changes to predict the rock fracture degree under different F-T environments. That is useful for fast loading-unloading and transporting coal or rock fragments.

5. Influence of F-T Temperature on the Microfracture Morphology

The mechanical properties and macrofracture characteristics of the rock mass are closely related to its microstructure. The scanning electron microscope (SEM) is used to reveal the microstructural characteristics of the yellow sandstone subjected to the different F-T temperatures from 20°C to −30°C. Figure 17 presents typical SEM surface images of specimen under different F-T temperatures. It should be noted that all SEM tests are performed before the impact testing. The results from the SEM are as follows:

(i) At the normal temperature, some initial pores, microcracks, and inconspicuous defects, which are closely related to the natural environment of yellow sandstone, are distributed within the rock. The internal matrix of the specimen is relatively dense. After the F-T treatment, some obvious defects (including pore cluster, larger holes, and interconnected cracks) are found in the interior of specimens that results in the strength weakening of rock as the density decreased.

(ii) SEM tests (magnification 1000) indicate that the F-T temperature has substantial influence on the microstructure of specimens. As the F-T temperatures drop from −5°C to −30°C, the internal defects of the specimens obviously increase, and the diameter of pores gradually expands (Figures 17(c) and 17(e)) and the crack width also dramatically increases (Figures 17(c) to 17(f)). The maximum crack widths

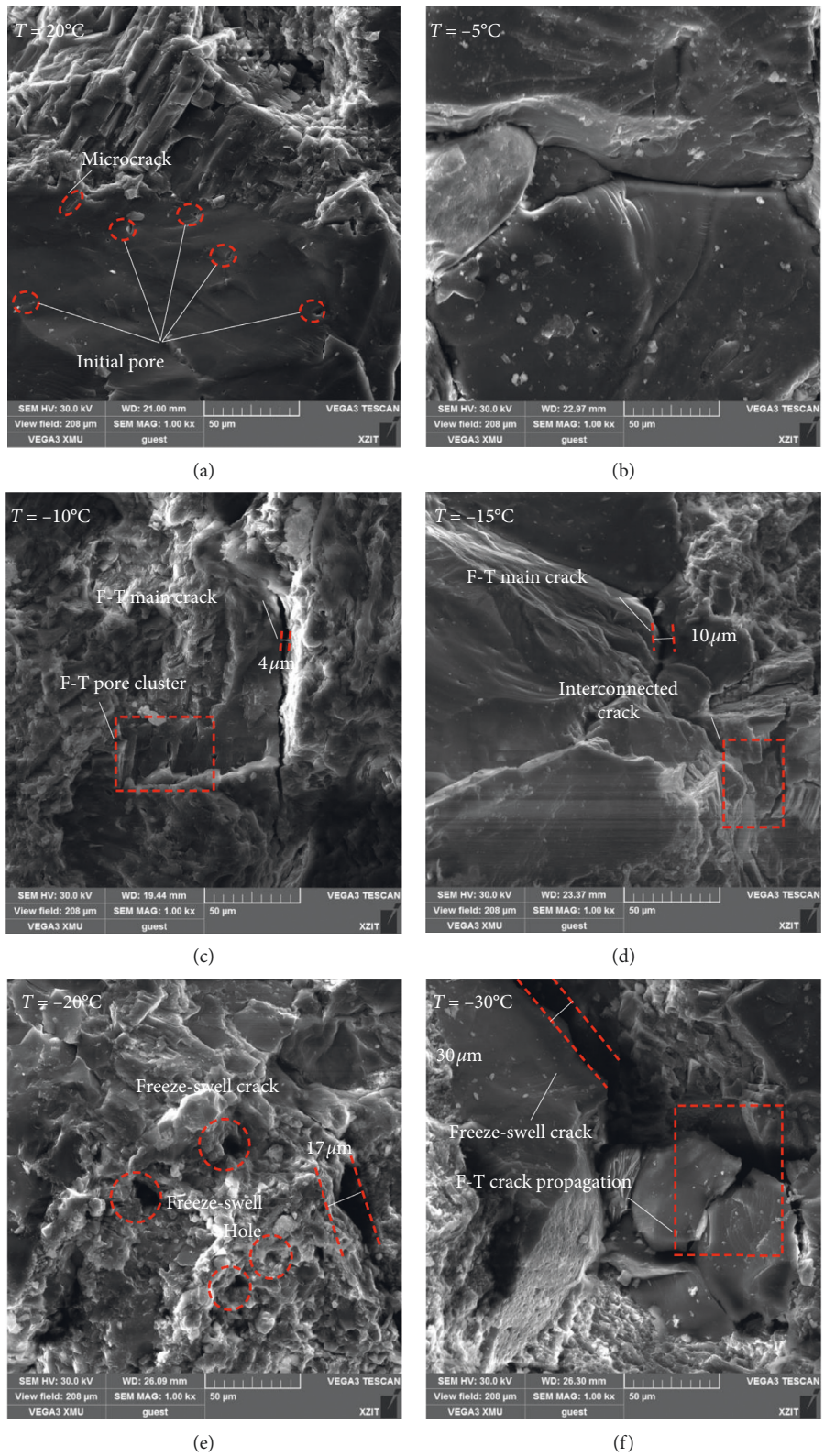

Figure 17: Microstructural characteristics of yellow sandstone under different F-T temperatures.

observed in the test samples are 4 μm for −10°C, 10 μm for −15°C, 17 μm for −20°C, and 30 μm for −30°C, respectively. When the F-T temperature reaches −15°C, the interconnected crack will be formed as shown in Figure 17(d). As the temperature continues to decrease, the freeze-swell holes cluster

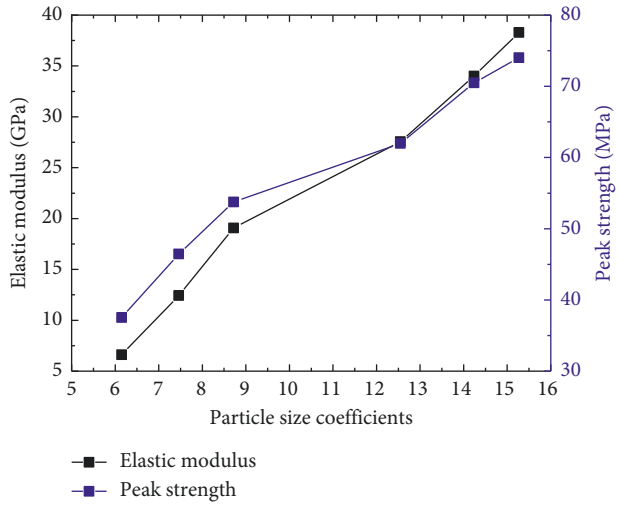

Figure 18: Relationship among particle size coefficient and elastic modulus as well as peak strength.

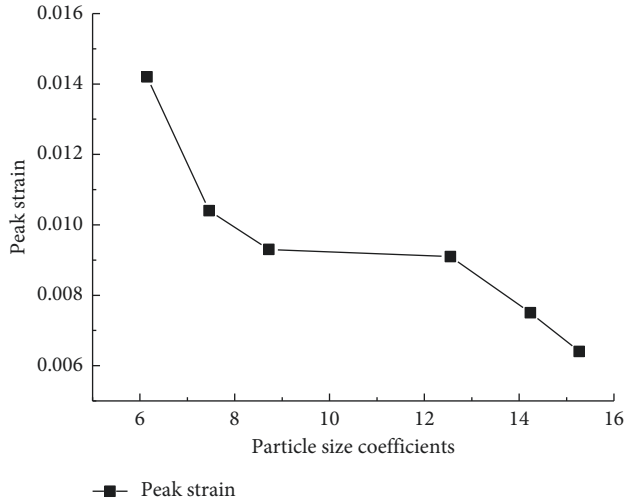

Figure 19: Relationship between particle size coefficient and peak strain.

are generated inside the yellow sandstone. Once the F-T temperature reaches −30°C, the larger size freeze-swell crack will appear and develop, which seriously damage the internal structure of the specimen.

As the F-T temperature decreases, the internal damage degree of the sample increases, which worsens its integrity and weakens the mechanical properties of rocks. The lumpiness distribution is also closely related to the specimen integrity. The higher the integrity of the sample, the less the number of small size particles. It means that the particle size coefficients gradually increase with the increasing F-T temperature, which is consistent with the conclusion in Section 4.

6. Influence of F-T Temperature on Energy Dissipation

6.1. Energy Dissipation Calculation. Based on the one-dimensional stress wave theory and the uniform stress assumption [27], with the incident wave, reflected wave, and transmitted wave measured by the high dynamic strain indicator, the stress ($\sigma(t)$), strain ($\varepsilon(t)$), and strain rate ($\dot{\varepsilon}(t)$) of the saturated yellow sandstone can be deduced through a three-wave analysis [28]:

$$\begin{cases} \sigma(t) = \dfrac{A_0 E_0}{2A_c}\left[\varepsilon_{\mathrm{I}}(t) - \varepsilon_{\mathrm{R}}(t) - \varepsilon_{\mathrm{T}}(t)\right], \\ \varepsilon(t) = \dfrac{C_0}{l_c}\displaystyle\int_0^t \left[\varepsilon_{\mathrm{I}}(t) - \varepsilon_{\mathrm{R}}(t) - \varepsilon_{\mathrm{T}}(t)\right]\mathrm{d}t, \\ \dot{\varepsilon}(t) = \dfrac{C_0}{l_c}\left[\varepsilon_{\mathrm{I}}(t) - \varepsilon_{\mathrm{R}}(t) - \varepsilon_{\mathrm{T}}(t)\right], \end{cases} \tag{2}$$

where $\varepsilon_{\mathrm{I}}(t)$, $\varepsilon_{\mathrm{R}}(t)$, and $\varepsilon_{\mathrm{T}}(t)$ are the strains of incident wave, reflected wave, and transmitted wave, respectively. E_0, A_0, and C_0 are Young's modulus, the cross-sectional area, and elastic longitudinal wave speed of the bar, respectively.A_c

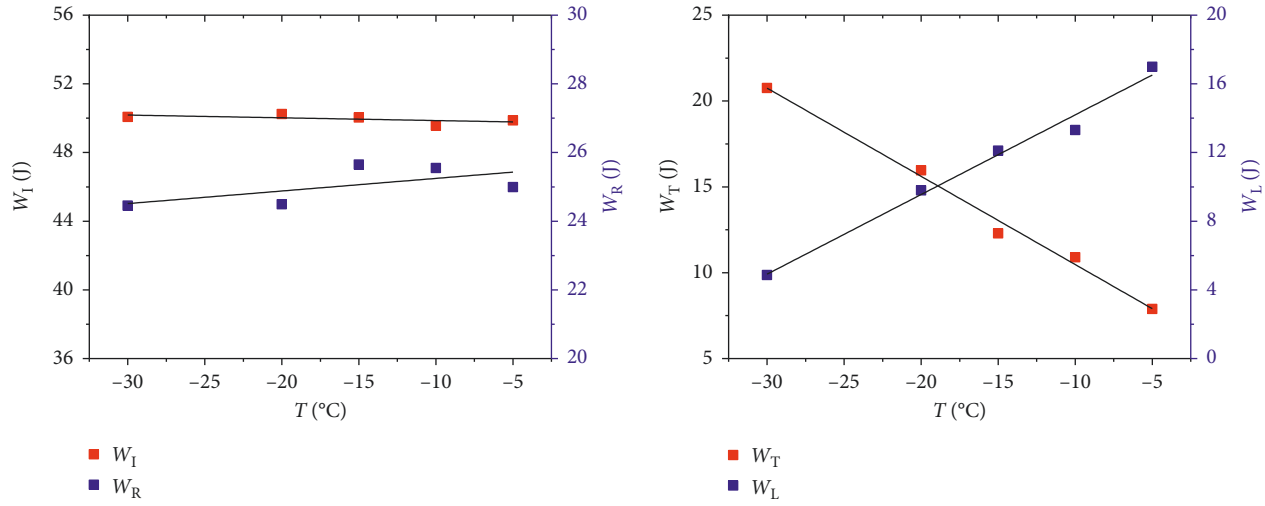

Figure 20: Variation regularity of energy dissipation with different F-T temperatures.

and l_c are the cross-sectional area and height of specimens, respectively.

Then, the incident energy (W_I), reflected energy (W_R), and transmitted energy (W_T) of the yellow sandstone can be calculated [28] as follows:

$$W_i = \begin{cases} \dfrac{A_0 C_0}{E_0} \displaystyle\int_0^t \sigma_I^2(t)\mathrm{d}t = E_0 A_0 C_0 \int_0^t \varepsilon_I^2(t)\mathrm{d}t, \\ \dfrac{A_0 C_0}{E_0} \displaystyle\int_0^t \sigma_R^2(t)\mathrm{d}t = E_0 A_0 C_0 \int_0^t \varepsilon_R^2(t)\mathrm{d}t, \\ \dfrac{A_0 C_0}{E_0} \displaystyle\int_0^t \sigma_T^2(t)\mathrm{d}t = E_0 A_0 C_0 \int_0^t \varepsilon_T^2(t)\mathrm{d}t, \end{cases} \tag{3}$$

where $\sigma_I(t)$, $\sigma_R(t)$, and $\sigma_T(t)$ are the incident wave stress, reflected wave stress, and transmitted wave stress, respectively.

The incident energy (W_i) caused by the impact between the incident bar and striker bar is mainly from four sources: the energy absorbed by the specimen, the energy reflected back into the incident bar, the energy propagated to the transmitted bar, and dissipated energy caused by the friction between the specimen and the bar, which accounts for a small proportion and can be ignored [27]. Hence, the dissipated energy (W_L) can be obtained by

$$W_L = W_I - W_R - W_T. \tag{4}$$

6.2. Energy Dissipation. The incident, reflected, transmitted, and dissipation energies of the yellow sandstone subjected to different F-T temperatures can be obtained by combining equations (3) and (4). Figure 20 presents the relationship between different energies and F-T temperatures. Both the incident energy and the reflected energy remain nearly unvaried as the F-T temperature gradually decreases. The incident energy and the reflected energy are in the range of 49.57–50.24 J with the average value 49.96 J and 24.45–25.65 J with the average value 25.03 J, respectively. However, the F-T temperature highly affects the transmitted and dissipation energies. As the F-T temperature drops from −5°C to −30°C, the transmitted energy increases linearly from 7.89 J to 20.76 J with an increasing rate of 163.12%, whereas the dissipation energy decreases linearly from 16.99 J to 4.86 J with a reduction rate of 71.39%. The relation between dissipation energy or transmitted energy and the F-T temperature can be, respectively, expressed as

$$\begin{cases} W_T = 18.83 + 0.46TR^2 = 0.9815, \\ W_L = 5.34 - 0.51TR^2 = 0.9883, \end{cases} \tag{5}$$

where W_T and W_L are transmitted energy and dissipated energy, respectively. The mechanism underlying this phenomenon can be interpreted as follows. The same impact load of 0.35 MPa is applied to all the saturated specimens of the yellow sandstone. Hence, the incident energy caused by the impact loading is approximately equal under different F-T temperatures. Based on the stress wave propagation theory, the reflection and transmission occur when the stress wave is transmitted to the interface between the incident bar and the specimen, and their values depend only on the wave impedance difference of materials and the contact state. In this F-T test, the F-T treatment led to the change in wave impedance difference of the yellow sandstone, whereas the reflection energy remains almost unvaried. That is mainly because the contact state between the specimen and the bar varied during the impact process.

In addition, as the F-T temperature declined, the inoculation, germination, extension, and penetration of the microcrack inside the sample accelerate the damage degree of the specimen, which leads to the degradation of the physical and mechanical properties of the rock. The propagation of initial cracks, expansion of pores, and the generation of new cracks consume energy to develop fracture

and promote the expansion of internal cracks. It should be noted that the energy dissipation decreases with an increasing porosity of the specimen [30]. Nevertheless, the F-T temperature can increase the damage degree and improve the porosity of rocks by the frost heaving effect [25, 29]. The deformation resistance ability of specimen is also weakened so that the dissipation energy absorbed by the specimen during the impact fracture process gradually decreases as the F-T temperature decreases. Hence, the transmitted energy collected by the impact test system will increase following equation (3).

7. Conclusions

In this work, a series of dynamic compression tests on the saturated yellow sandstone subjected to different F-T temperatures (i.e., −5°C, −10°C, −15°C, −20°C, −30°C, and 20°C) are carried out using SHPB equipment with eight F-T cycle numbers. The coupling effect of the F-T temperature and impact load on the mechanical properties, lumpiness distribution, microstructural feature, and energy dissipation of the specimens is discussed. From the investigation, the following conclusions can be drawn:

(i) Under the same strain rate, as the F-T temperature gradually decreased, both the *P*-wave velocity and the density of the saturated specimens decreased. The dynamic elastic modulus and peak strength also decreased, whereas the dynamic peak strain increased. Meanwhile, the specimen transitioned from brittle behavior to ductile behavior.

(ii) When the strain rate is in the range of 72.88 s^{-1} to 75.97 s^{-1}, the fracture modes of the yellow sandstone mainly include the double-cone failure pattern, single-side slope failure pattern, double-side slope failure pattern, and split failure pattern. The particle size coefficient markedly decreased from −5°C to −20°C with a high gradient while decreased gradually from 20°C to −5°C and −20°C to −30°C with a lower speed rate. Hence, the effect of the F-T temperature on the macroscopic fracture degree of the yellow sandstone is significant, particularly in the range of −20°C to −5°C.

(iii) SEM analysis shows that the F-T temperature is able to contribute to the internal damage degree of the specimen and produces a high number of freeze-swell holes, interconnected cracks, pores cluster, and other defects inside the specimen. Both the pore diameter and crack width gradually increased with the decrease of the F-T temperature. The fragment size caused by the impact tests gradually decreased. This is consistent with the macrofracture characteristics of the yellow sandstone.

(iv) As the F-T temperature decreased, both the incident and reflected energies remain approximately constant whereas the transmitted energy increased linearly and the dissipation energy decreased linearly.

Data Availability

The data used to support the findings of this study are available from the corresponding author upon request.

Conflicts of Interest

The authors declare that there are no conflicts of interest regarding the publication of this paper.

Acknowledgments

This work was supported by the Fundamental Research Funds for the Central Universities (2018BSCXB20) and the Postgraduate Research & Practice Innovation Program of Jiangsu Province (KYCX18_1968).

References

[1] J. Zhang, H. Deng, A. Taheri, and C. Liu, "Deterioration and strain energy development of sandstones under quasi-static and dynamic loading after freeze-thaw cycles," *Cold Regions Science and Technology*, vol. 160, pp. 252–264, 2019.

[2] F. Q. Gong, D. H. Lu, X. B. Li, and Q.-H. Rao, "Experimental research of sandstone dynamic strength criterion under different strain rates," *Rock and Soil Mechanics*, vol. 34, no. 9, pp. 2433–2441, 2013.

[3] A. Taheri, N. Yfantidis, C. Olivares, B. J. Connelly, and T. J. Bastian, "Experimental study on degradation of mechanical properties of sandstone under different cyclic loadings," *Geotechnical Testing Journal*, vol. 39, no. 4, pp. 673–687, 2016.

[4] A. Taheri, A. Royle, Z. Yang, and Y. Zhao, "Study on variations of peak strength of a sandstone during cyclic loading," *Geomechanics and Geophysics for Geo-Energy and Geo-Resources*, vol. 2, no. 1, pp. 1–10, 2016.

[5] H. Zhao and A. Taheri, "Local damage and progressive localisation in porous sandstone during cyclic loading," *Rock Mechanics and Rock Engineering*, vol. 50, no. 12, pp. 3253–3259, 2017.

[6] H. Munoz and A. Taheri, "Post-peak deformability parameters of localised and non-localised damage zones of rocks under cyclic loading," *Geotechnical Testing Journal*, vol. 42, no. 6, p. 22, 2019.

[7] Y. C. Li, S. Y. Sun, and C. A. Tang, "Analytical prediction of the shear behaviour of rock joints with quantified waviness and unevenness through wavelet analysis," *Rock Mechanics and Rock Engineering*, pp. 1–13, 2019.

[8] Z. Zhou, W. Ma, S. Zhang, Y. Mu, and G. Li, "Effect of freeze-thaw cycles in mechanical behaviors of frozen loess," *Cold Regions Science and Technology*, vol. 146, pp. 9–18, 2018.

[9] T. C. Chen, M. R. Yeung, and N. Mori, "Effect of water saturation on deterioration of welded tuff due to freeze-thaw action," *Cold Regions Science & Technology*, vol. 38, no. 2-3, pp. 127–136, 2004.

[10] A. Saad, S. Guédon, and F. Martineau, "Microstructural weathering of sedimentary rocks by freeze-thaw cycles: experimental study of state and transfer parameters," *Comptes Rendus Geoscience*, vol. 342, no. 3, pp. 197–203, 2010.

[11] H. Yavuz, "Effect of freeze-thaw and thermal shock weathering on the physical and mechanical properties of an andesite stone," *Bulletin of Engineering Geology and the Environment*, vol. 70, no. 2, pp. 187–192, 2011.

[12] X. Tan, W. Chen, J. Yang, and J. Cao, "Laboratory investigations on the mechanical properties degradation of granite under freeze-thaw cycles," *Cold Regions Science and Technology*, vol. 68, no. 3, pp. 130–138, 2011.

[13] A. Özbek, "Investigation of the effects of wetting-drying and freezing-thawing cycles on some physical and mechanical properties of selected ignimbrites," *Bulletin of Engineering Geology and the Environment*, vol. 73, no. 2, pp. 595–609, 2014.

[14] M. Fener and İ. İsmail, "Effects of the freeze-thaw (F-T) cycle on the andesitic rocks (Sille-Konya/Turkey) used in construction building," *Journal of African Earth Sciences*, vol. 109, pp. 96–106, 2015.

[15] İ. İsmail and M. Fener, "A prediction model for uniaxial compressive strength of deteriorated pyroclastic rocks due to freeze–thaw cycle," *Journal of African Earth Sciences*, vol. 120, pp. 134–140, 2016.

[16] J. Eslami, C. Walbert, A.-L. Beaucour, A. Bourges, and A. Noumowe, "Influence of physical and mechanical properties on the durability of limestone subjected to freeze-thaw cycles," *Construction and Building Materials*, vol. 162, pp. 420–429, 2018.

[17] X. Luo, N. Jiang, C. Zuo, Z. Dai, and S. Yan, "Damage characteristics of altered and unaltered diabases subjected to extremely cold freeze-thaw cycles," *Rock Mechanics and Rock Engineering*, vol. 47, no. 6, pp. 1997–2004, 2014.

[18] A. Al-Omari, K. Beck, X. Brunetaud, Á. Török, and M. Al-Mukhtar, "Critical degree of saturation: a control factor of freeze-thaw damage of porous limestones at Castle of Chambord, France," *Engineering Geology*, vol. 185, pp. 71–80, 2015.

[19] L. Wen, X. B. Li, Q. H. Wu, L. Weng, and W. Su, "Dynamic strength of granite porphyry under freezing-thawing cycles," *Chinese Journal of Rock Mechanics & Engineering*, vol. 34, no. 7, pp. 1297–1306, 2015.

[20] N. G. Yang, K. P. Zhou, T. Lei, J. Li, and F. Bin, "Sandstones dynamic mechanical properties and failure characteristics under freeze-thaw cycles," *Chinese Journal of Nonferrous Metals*, vol. 26, no. 10, pp. 2181–2187, 2016.

[21] K.-P. Zhou, B. Li, J.-L. Li, H.-W. Deng, and F. Bin, "Microscopic damage and dynamic mechanical properties of rock under freeze-thaw environment," *Transactions of Nonferrous Metals Society of China*, vol. 25, no. 4, pp. 1254–1261, 2015.

[22] B. Ke, K. Zhou, H. Deng, and F. Bin, "NMR pore structure and dynamic characteristics of sandstone caused by ambient freeze-thaw action," *Shock and Vibration*, vol. 2017, Article ID 9728630, 10 pages, 2017.

[23] J. Bin, R. B. Kaunda, and K. Zhou, "Experimental investigations on the effects of ambient freeze-thaw cycling on dynamic properties and rock pore structure deterioration of sandstone," *Cold Regions Science and Technology*, vol. 154, pp. 133–141, 2018.

[24] J. Ruedrich, D. Kirchner, and S. Siegesmund, "Physical weathering of building stones induced by freeze–thaw action: a laboratory long-term study," *Environmental Earth Sciences*, vol. 63, no. 7-8, pp. 1573–1586, 2011.

[25] W. T. Liao, H. Q. Zhu, Y. Yang, Y. Wu, and Y. Fan, "Study on low temperature mechanical properties of rocks under high strain rate," *Revista de la Facultad de Ingeniería UCV*, vol. 31, no. 5, pp. 197–208, 2016.

[26] C. E. Fairhurst and J. A. Hudson, "Draft ISRM suggested method for the complete stress–strain curve for intact rock in uniaxial compression," *International Journal of Rock Mechanics & Mining Sciences*, vol. 36, no. 3, pp. 281–289, 1999.

[27] Q. Ma, D. Ma, and Z. Yao, "Influence of freeze-thaw cycles on dynamic compressive strength and energy distribution of soft rock specimen," *Cold Regions Science and Technology*, vol. 153, pp. 10–17, 2018.

[28] M. Li, X. Mao, L. Cao, H. Pu, and A. Lu, "Influence of heating rate on the dynamic mechanical performance of coal measure rocks," *International Journal of Geomechanics*, vol. 17, no. 8, pp. 1–11, 2017.

[29] X. Fang, J. Xu, and P. Wang, "Compressive failure characteristics of yellow sandstone subjected to the coupling effects of chemical corrosion and repeated freezing and thawing," *Engineering Geology*, vol. 233, pp. 160–171, 2018.

[30] C. J. Xia, H. P. Xie, Y. Ju, and H.-W. Zhou, "Experimental study of energy dissipation of porous rock under impact loading," *Engineering Mechanics*, vol. 23, no. 9, pp. 1–5, 2006.